

Measurement of tensor polarization of deuterons from ${}^3\text{He} \rightarrow d + p$ breakup at momenta from 4.60 to 5.66 GeV/c

I. M. Sitnik,^{1,*} C. F. Perdrisat,² E. Tomasi-Gustafsson,^{3,4} J. Ball,^{3,4} L. Bimbot,⁵ Y. Bisson,⁵ M. Boivin,³ Yu. T. Borzunov,¹ J. L. Boyard,⁵ Ph. Courtat,⁵ R. Gacougnolle,⁵ L. B. Golovanov,¹ T. Hennino,⁵ M. K. Jones,⁶ R. Kunne,⁵ L. V. Malinina,¹ S. Nedev,⁷ N. M. Piskunov,¹ V. Punjabi,⁸ J. L. Sans,³ R. Skowron,⁵ E. A. Strokovsky,¹ and J. Yonnet³

¹Joint Institute for Nuclear Research, RU-141980 Dubna, Russia

²College of William and Mary, Williamsburg, Virginia 23187, USA

³CEA/DSM CNRS/IN2P3 Laboratoire National Saturne, CE Saclay, France

⁴DAPNIA/SPHN CEA/Saclay, F-91191 Gif-sur-Yvette Cedex, France

⁵CNRS/IN2P3 IPN, F-91400 Orsay, France

⁶Thomas Jefferson National Accelerator Facility, Newport News, Virginia 23606, USA

⁷University of Chemical Technology and Metallurgy, Sofia, Bulgaria

⁸Norfolk State University, Norfolk, Virginia 23504, USA

(Received 20 April 2011; revised manuscript received 17 July 2011; published 19 September 2011)

The tensor polarization ρ_{20} of deuterons emitted in the ${}^1\text{H}({}^3\text{He}, \vec{d})X$ reaction at 0° in the laboratory system was measured at the Saturne National Laboratory in Saclay using the SPES-4 spectrometer with the HYPOM polarimeter located downstream from its focal plane. The momentum of the detected deuterons was kept fixed at 3.77 GeV/c, while the momentum of the ${}^3\text{He}$ beam was varied from 4.60 to 5.66 GeV/c, thus providing a range of internal momenta k of the deuteron in ${}^3\text{He}$ from 0 up to 0.4 GeV/c. The data obtained are compared with theoretical predictions.

DOI: [10.1103/PhysRevC.84.034006](https://doi.org/10.1103/PhysRevC.84.034006)

PACS number(s): 21.45.-v, 24.70.+s, 13.88.+e, 25.10.+s

I. INTRODUCTION

Disintegration of the lightest nuclei is an effective tool for the study of few-body systems in nuclear physics. The study of the ${}^3\text{He}$ breakup reactions into various channels with nuclear probes in the intermediate-energy region started in 1972 at the Space Radiation Effects Laboratory (SREL) [1] and continued at TRIUMF [2]. Inclusive measurements of ${}^{12}\text{C}({}^3\text{He}, d)X$ and ${}^{12}\text{C}({}^3\text{He}, p)X$ at a ${}^3\text{He}$ momentum of 10.7 GeV/c were performed for the first time in Dubna with the ALPHA spectrometer [3] in a wide region of internal momenta of the fragments. The ultimate goal of all these experiments was to get experimental information about the momentum distribution of nucleons in the ${}^3\text{He}$ nucleus and compare it with theoretical predictions. Results of these experiments have been consistent in the region of internal momenta of nucleons in ${}^3\text{He}$ where the explored momentum regions overlapped, while at higher momenta unexpected behavior of the fragment spectra was observed [3]. That was the first step of a program aimed at the study of the ${}^3\text{He}$ structure at moderate and short distances between constituents. The next step in experimental studies of the ${}^3\text{He}$ structure had to include relevant spin-dependent observables, as became clear from investigations of the structure of the deuteron [4–6]. It was demonstrated in those experimental studies that spin-dependent observables bring very important and new information. It was shown, for example, that none of the existing theoretical models could provide a good self-consistent description of the cross sections and spin-dependent observables simultaneously. Moreover, all

models which are relatively successful in describing cross sections fail when applied to spin-dependent data.

A number of relevant single and double spin-dependent observables for the ${}^3\text{He}$ case were theoretically considered in Ref. [7]. Experiments with hadronic probes in the intermediate-energy region, measuring polarization observables, started recently.

The first experiment in the intermediate-energy region, where double spin-dependent variables were measured and the ${}^3\text{He}$ structure was studied using hadron probes, was done at Osaka University [8]. In this experiment the spin correlation parameter C_{yy} was measured in backward elastic ${}^3\text{He}(\vec{p}, {}^3\text{He})p$ reaction in the 200 to 400 MeV energy interval.

Here we present the final results of another experiment where a single-spin observable was measured; namely, the tensor polarization of the deuterons (ρ_{20}) emitted at zero degrees in the ${}^1\text{H}({}^3\text{He}, \vec{d})X$ breakup reaction with unpolarized ${}^3\text{He}$ and an unpolarized hydrogen target. In this case, only tensor deuteron polarization may be different from 0, as follows from the symmetry laws. The Feynman graphs of the investigated process in the plane-wave impulse approximation (PWIA) are shown in Fig. 1.

This experiment exploits the so-called double scattering method of measurements, which means that, in the first (production) interaction, a particle is produced whose polarization is analyzed in a subsequent (analyzing) scattering from a second target in a polarimeter. The measurements presented here were performed at the Saturne National Laboratory in Saclay, using the SPES-4 spectrometer and the HYPOM polarimeter [9] located downstream of the focal plane of SPES-4. The polarimeter contained an LH₂ target to take

*sitnik@dubna.ru

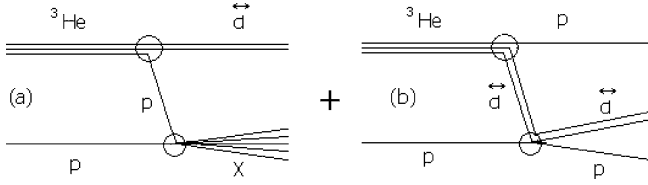


FIG. 1. Feynman graphs for the studied process in the framework of PWIA. (a) Deuteron-spectator + elastic and inelastic pp interaction. (b) Proton-spectator + elastic dp scattering.

advantage of the large analyzing power T_{20} of elastic dp scattering [10] within the diffractive cone.

In the ${}^3\text{He}$ rest frame the deuteron fragment has momentum $q \simeq 0$ when its momentum in the laboratory system is $p_d = 2/3 p_{{}^3\text{He}}$. This experiment was performed in the range of $p_d > 2/3 p_{{}^3\text{He}}$. The tune of the SPES-4 spectrometer, which transferred the deuterons produced in the ${}^1\text{H}({}^3\text{He}, \vec{d})X$ reaction to the analyzer in the HYPOM polarimeter, was kept fixed at a momentum of 3.77 GeV/c, while the ${}^3\text{He}$ beam momentum was varied from 5.66 to 4.60 GeV/c. This method of keeping the momentum of the analyzed particle fixed was used previously in measurements of the polarization transfer from vector polarized deuteron to its fragment (proton) in ${}^{12}\text{C}(\vec{d}, \vec{p})X$ [6]. It allows us to avoid systematic errors due to the energy dependence of the analyzing power in the analyzing reaction $dp \rightarrow dp$ when the momentum of the analyzed particle varies. Instead, it assumes independence of the measured quantity from the projectile momentum. Such an implicit assumption seems to be justified in the deuteron case [4,6] by the experimentally verified fact of the independence of other observables (cross sections and tensor analyzing power) from the projectile energy.

The main difficulties of this experiment are related to the facts that it was not possible to alternate the sign of the deuteron polarization to minimize residual asymmetries and that the absence of an azimuthal asymmetry in the deuteron production reaction, which is because there is no reaction plane since the initial and the final particle momenta are collinear.

The asymmetry produced by the tensor polarization of the deuterons emitted in the breakup of unpolarized ${}^3\text{He}$ was obtained from a comparison of the t dependence (t is the Mandelstam four-momentum transfer squared) of the yields in the analyzed scattering with the “reference” yields measured in calibrating runs with an unpolarized deuteron beam. In order to keep systematic errors under control and at an acceptable level, the time drifts of the calibration constants of the polarimeter had to be investigated very carefully.

II. EXPERIMENTAL SETUP AND CHARACTERISTICS OF DATA

A. Elements of setup

The extracted beam of ${}^3\text{He}$ nuclei from SATURNE II was transported to the SPES-4 spectrometer facility. The breakup reaction ${}^1\text{H}({}^3\text{He}, d)X$, with emission of a deuteron at 0° in the laboratory system, took place in a 10 cm LH_2 target installed inside the TETHYS dipole, located directly upstream of the

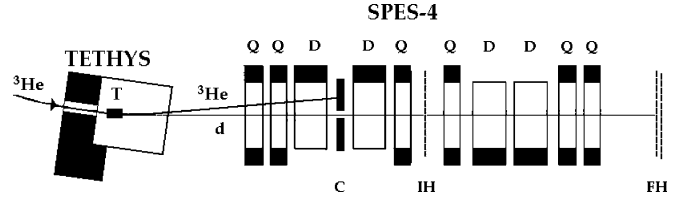


FIG. 2. Schematic top view of SPES-4 spectrometer. D indicates dipoles, Q indicates quadrupoles, T indicates first LH_2 target, C indicates the collimator, and IH and FH are intermediate and final focal-plane hodoscopes, respectively.

SPES-4 spectrometer [11]. The deuterons were transported by the SPES-4 optical system to the polarimeter HYPOM [9]. The focusing A mode [11] with angular acceptance within ± 40 mrad was used.

The main components of the SPES-4 spectrometer are shown in Fig. 2. The hodoscopes IH and FH , located at the intermediate and final focal planes, formed the time-of-flight (TOF) system of the spectrometer. The IH hodoscope contained one row of 12 scintillation counters; the FH hodoscope consisted of two rows of overlapping counters (12 per row).

The set of detectors in the final focal plane, together with the HYPOM polarimeter, is shown in Fig. 3. Apart from the FH hodoscope, this set included the standard SPES-4 trackers (multi-wire proportional chambers, or MWPC) and two large overlapping counters S_1 – S_2 of size $(x : 500) \times (y : 200) \times (z : 10)$ mm³; the overlap was 20 mm along the Y axis to match the vertical size of the cells of the analyzing target. Here the Z axis coincides with the optical axis of the spectrometer and is directed downstream, the Y axis is directed vertically in the “up” direction, and the X axis is in the horizontal plane so as to form a right-handed coordinate system.

The deuterons have to be scattered by the analyzing target of the polarimeter to allow for a trigger to be formed. Their spatial distribution in the horizontal plane (XZ) was rather wide because of the high dispersion of SPES-4 (Fig. 4). In order to match it, a special LH_2 target [12] containing two elements was built specifically for this experiment. The size of each target element was $(x : 500) \times (y : 20) \times (z : 100)$ mm³. The size of the cells in the Y direction determined the acceptance of the spectrometer in that direction. A tomographical picture of the target is shown in Fig. 5.

The scattered deuterons were detected by the MWPC of the HYPOM polarimeter with the RH hodoscope behind them.

The angular coefficient of the recoil proton track (i.e., $a_s = dz/dy$) was measured by (3 + 1) straw-tube planes located parallel to the (XZ) plane above and beneath the analyzing target. Each straw tube plane had 32 tubes 500 mm in length and 10.9 mm in diameter directed parallel to the global X axis.

The detectors surrounding the target were followed by four sets of two scintillation counters S_3 – S_{10} with thicknesses of 3 and 12 mm, respectively. Their xz sizes were 500×160 mm². The counters were used to measure the recoil particle energies.

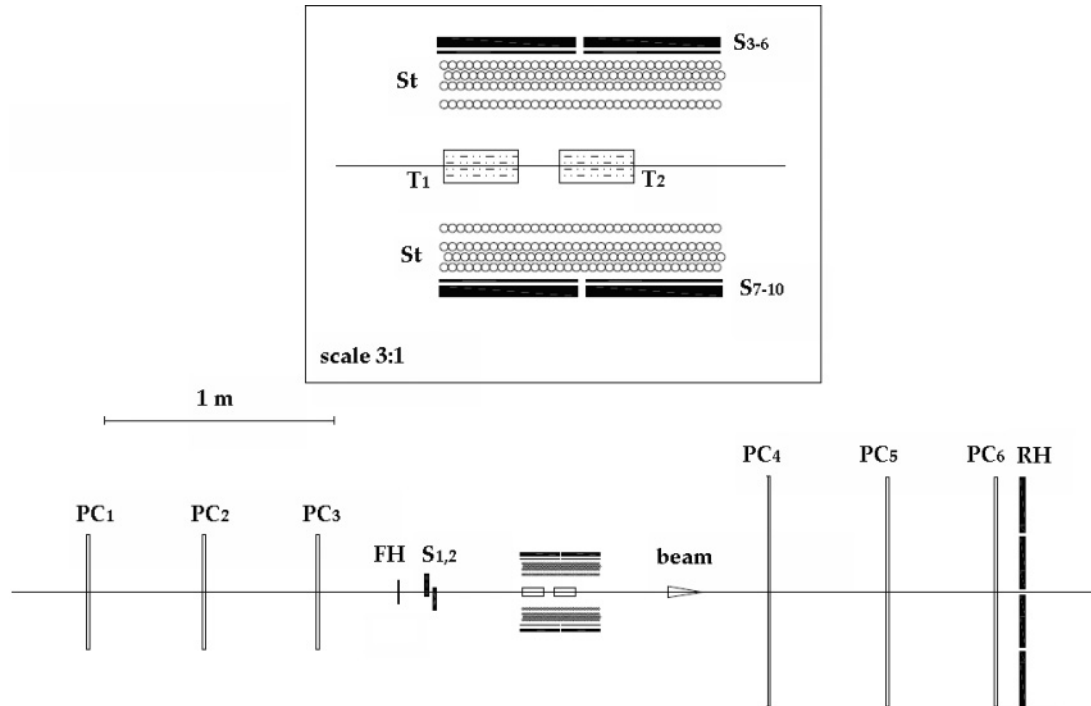


FIG. 3. Schematic side view of polarimeter. S_i indicates scintillator counters, PC_i indicates proportional chambers, T_i indicates LH_2 targets, St indicates straws, and FH and RH indicate final focal-plane and rear hodoscopes, respectively.

B. Trigger

The first-stage trigger of the setup was designed to ensure that the deuteron, transported to the polarimeter from the production target, passed through the target and all the trackers of the polarimeter. This was obtained by requiring coincidences of signals from the FH hodoscope, the S_1 – S_2 counters, and the RH hodoscope.

Elastic scattering candidate events were selected with the help of the second-stage trigger (the recoil trigger), which

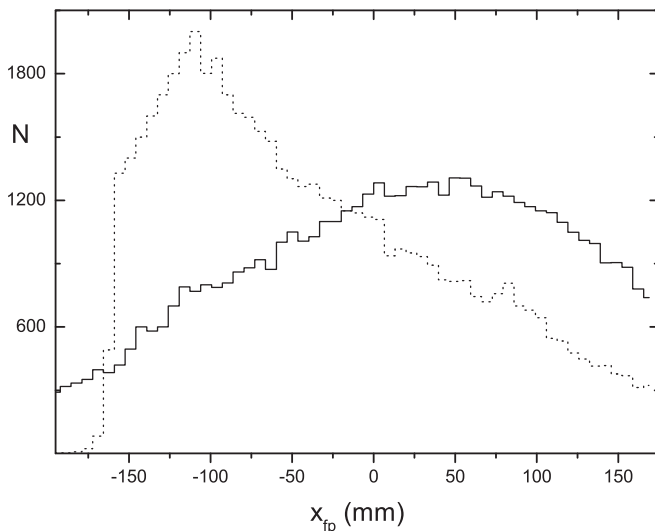


FIG. 4. x distribution of the beam particles at the focal plane for $q \simeq 0$ (solid line) and for $q \gg 0$ (dashed line).

required a coincidences in at least one pair of the scintillation counter sets S_3 – S_{10} .

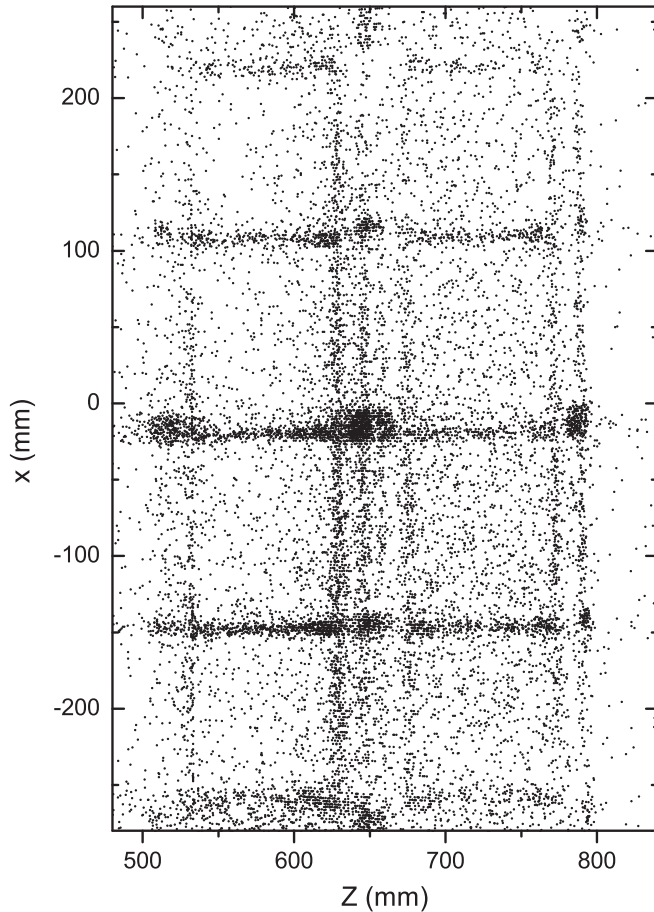
C. Data-taking details

Measurements of the tensor polarization of the deuterons produced in the reaction $^1\text{H}(^3\text{He},d)X$ with unpolarized ^3He were carried out at the incident ^3He beam momenta of 5.66, 5.07, 4.90, 4.74, and 4.60 GeV/ c . The tune of the SPES-4 transport line was kept fixed at a central deuteron momentum p_0 of the deuteron of 3.77 GeV/ c ; the relative momentum acceptance of the beam transport line was $\Delta p/p_0 \simeq 0.025$. In order to verify that the tuning procedure resulted in the same value of the deuteron “central momentum,” the data from the SPES-4 TOF system were used to check the average value of p_0 at each setting.

Because the first target was installed inside a dipole (TETHYS), each change of the ^3He beam energy required a change of the target position as well as introduction of a correction to the SPES-4 tune in order to keep particles with central SPES-4 momentum ($p_0 = 3.77$ GeV/ c) at the optical axis of the spectrometer. In other words, single charged particles with fixed momentum p_0 had to be transported to the fixed ($x = 0$) position in the focal plane. The necessary corrections were applied automatically by use of a special computer code.

The beam intensity was chosen at a level resulting in an acceptably low (not more than 15%) dead time of the polarimeter.

When the measurements were performed at the largest value of q , the rightmost (high-momentum side at the SPES-4 focal

FIG. 5. zx distribution of interaction points.

plane) 3 counters of the FH hodoscope were switched off. This resulted in suppression of a substantial background of tritons at the polarimeter detector, produced in inelastic $^1\text{H}(^3\text{He}, t)X$ charge exchange at the production target.

The polarimeter HYPOM had to be calibrated because the tensor analyzing power of the elastic dp scattering was previously known only up to 2.93 GeV/ c [10]. The polarized deuteron beam used for calibration was provided by the Hyperion ion source [13,14]. The standard nomenclature of the source modes for production of a tensor polarized deuteron beam is given in Table I. The source ran sequentially through modes 5 to 8. Each spill of the accelerated beam was labeled in accordance with the corresponding mode of the Hyperion source.

The calibration was done at two values of the deuteron beam momenta: $p_{d, \text{calibr}} = 3.77$ and $p_{d, \text{calibr}} = 3.39$ GeV/ c . This was necessary because the average momentum of the analyzed deuterons, fragments of the ^3He , was typically less

TABLE I. Extremum values of the beam polarizations in the used Hyperion modes.

Mode	5	6	7	8
P_z	+1/3	-1/3	+1/3	-1/3
P_{zz}	+1	+1	-1	-1

than the central momentum p_0 of SPES-4, except for the region $q \simeq 0$ (Fig. 4).

The deuteron beam polarization was measured with the standard SATURNE-II polarimeters and was found to be of $P_{zz} = 0.82 \pm 0.03$ and 0.79 ± 0.04 at 3.77 and 3.39 GeV/ c , respectively.

III. EVENT RECONSTRUCTION

The polar and azimuthal scattering angles (θ, φ) of the incident particles relative to the HYPOM polarimeter were calculated from the front (particles hitting the analyzing target) and rear (scattered particle) MWPC. The momentum of the incident particle p was calculated from the front trackers and the SPES-4 optical constants. On the basis of the (p, θ, φ) information obtained, the expected value of the Mandelstam four-momentum transfer squared t and parameters of the recoil proton track and of the proton energy (marked below by symbol $'$) were predicted using elastic two-body kinematics. The (YZ) projections of the track of the recoil particles were measured by the recoil trackers (the straw planes). Their kinetic energy was measured by counters S_3 – S_{10} , as mentioned in Sec. II A.

The particles incident on the polarimeter target were identified with the help of the TOF information.

A. Reconstruction of tracks

The track parameters in the MWPC [15] were obtained from the relations

$$\begin{aligned} x &= a_{xm}z + b_{xm}, \\ y &= a_{ym}z + b_{ym}, \end{aligned} \quad (1)$$

where the index $m = f, r$ refers to the front and rear chambers, respectively. Tracks in the straws were fit according to equation

$$z = a_s y + b_s. \quad (2)$$

This procedure is described in detail in Appendix A. In this approach, the z coordinate of the interaction point, z_{int} , was obtained using information from the front trackers and straws as follows:

$$z_{\text{int}} = \frac{b_s + a_s b_{yf}}{1 - a_s a_{yf}}. \quad (3)$$

After that the interaction coordinates x_{int} and y_{int} were found by substitution of z_{int} into Eq. (1). A good resolution on the interaction point coordinates can be seen in Fig. 5, where concentrations of interaction points indicate the position of the target walls.

The coordinates of the interaction point obtained as explained above were used as additional input in search for tracks in the rear chambers PC_4 to PC_6 because of their lower efficiency and accuracy.

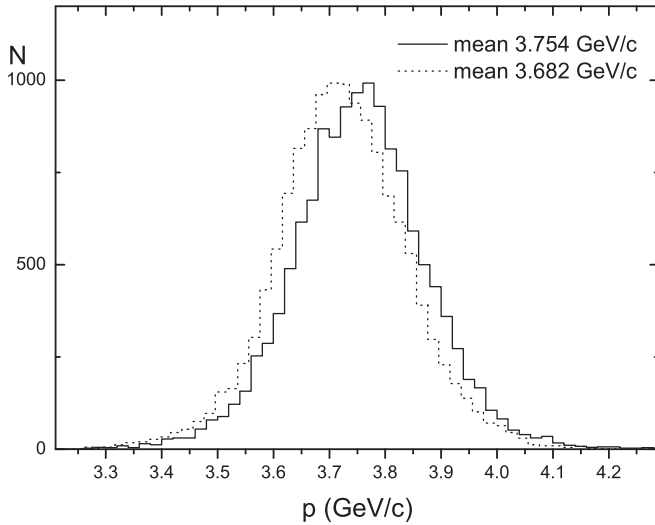


FIG. 6. Distributions of secondary beam momentum, from the central counters of the TOF system for two sets of data at $k = 0$ (solid line) and $k = 0.214$ GeV/c (dashed line).

B. Identification of deuterons and reconstruction of their momenta

At several incident momenta of ${}^3\text{He}$ the inelastic charge-exchange reaction ${}^3\text{He} + p \rightarrow t + X$ in the production target generated a significant admixture of tritons transported to the focal plane of SPES-4. Information from the TOF system was used to exclude these tritons. The corresponding raw TDC data were sufficient for this separation.

As mentioned in Sec. II, the production target was installed in the dipole and, at each setting of the ${}^3\text{He}$ momentum, the dipole current had to be readjusted in order to keep the position of the beam at the target fixed (Fig. 2) as well as to perform retuning of the SPES-4 line so as to have identical values of the central momentum of secondary deuterons (p_0). The TOF system was also used in this procedure to check the average value of p_0 . The coefficients transforming the raw TDC values to the particle velocities β were found on the basis of the calibration data taken with deuteron beams of two different momenta.

The deuteron momentum distributions, obtained from the central counters of the TOF system for two sets of ${}^1\text{H}({}^3\text{He}, d)$ data are shown in Fig. 6. As one can see from this figure, the statistics was sufficient to determine the average p_0 values, which are presented in Table II, with good accuracy. An

accurate value of p_0 is important in order to avoid systematical shifts in the calculated four-momentum transfer squared, t .

For data sets with $q \simeq 0$ the central momentum can be found independently: the position of the maximum in Fig. 4 takes place at $q = 0$ which is $p = 3.773$ GeV/c. The p_0 estimates obtained by both methods agree well, within the error bars.

The momentum of the deuterons hitting the HYPOM analyzing target was found from the relation

$$\frac{\Delta p}{p_0} = k_1 x + k_2 (a_{xf} - \langle a_{xf} \rangle),$$

$$p = \frac{p_0}{\left(1 - \frac{\Delta p}{p_0}\right)}, \quad (4)$$

where x is the deflection of the track from the z axis in the focal plane, and $\langle a_{xf} \rangle = k_3 x$ is the average value of a_{xf} for a given x . In our system of coordinates the focal plane is positioned at $z = 0$, so, $x = b_{xf}$. The k_1 and k_2 constants used were obtained in Ref. [16].

C. Estimation of recoil particle energy loss

The expected Analog to Digital Converter (ADC) values (s'_1, s'_2) from the counters S_3 to S_{10} , combined in pairs, were calculated on the basis of the estimated kinetic energy of the recoil particles, taking into account the corresponding energy losses in hydrogen and material between the hydrogen and the first of the counters. The flight path length in hydrogen was calculated from the y_{int} value in Eq. (3). The nonlinearity of the photomultipliers and the dependence of the signal upon the distance between the source of light and the photomultipliers were also taken into account.

A fraction of the recoil particles were stopped in the last (“thick”) counter of each pair of counters. For such particles, the “thick” counters served as the E detector and the corresponding pair was a ΔE - E detector. This occurred for $|t|$ values from $|t| \sim 0.085$ (GeV/c) 2 (azimuthal angle $\varphi \approx 90^\circ$) up to $|t| \sim 0.125$ (GeV/c) 2 (azimuthal angle $\varphi \approx 45^\circ$) depending on φ .

At higher values of $|t|$ the recoil protons punched through the “thick” counters and the corresponding pair served as an effective ΔE_1 - ΔE_2 detector. The energy-loss spectrum in one of the “thick” counters is shown in Fig. 7 as a function of t .

The main background process, quasielastic pp scattering, takes place when the proton momentum from the deuteron is (on average) half of the incident deuteron momentum. Because

TABLE II. Measured data on ρ_{20} in dependence on the k variable together with the kinematical parameters of the experiment.

Set Number	$p_{{}^3\text{He}}$ GeV/c	Triggers/ 10^3	p_0 GeV/c	$\langle p \rangle$ GeV/c	$\langle k \rangle$ GeV/c	σ_k	ρ_{20}
1	5.660	470	3.754 ± 0.04	3.776	0.021	0.013	0.008 ± 0.260
2	5.660	408	3.759 ± 0.03	3.776	0.018	0.013	0.131 ± 0.212
3	5.073	422	3.750 ± 0.04	3.689	0.178	0.027	-0.442 ± 0.176
4	4.900	837	3.682 ± 0.04	3.654	0.214	0.027	-0.628 ± 0.089
5	4.738	952	3.703 ± 0.03	3.688	0.305	0.035	-0.606 ± 0.100
6	4.598	1169	3.762 ± 0.03	3.749	0.398	0.041	-0.116 ± 0.138

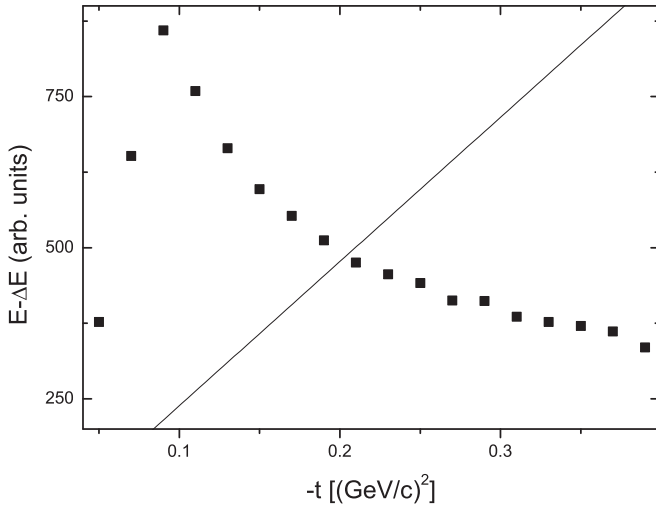


FIG. 7. ΔE - E losses in thick counters (solid squares). Calculated losses for the quasielastic pp scattering at the same laboratory angle at which the elastic dp scattering took place.

the kinetic energy of the recoil particle, T , is approximately proportional to $-t \simeq (H\theta)^2$ in elastic small-angle scattering, for the quasielastic scattering case (when the projectile proton scatters at the same angle as the projectile deuteron) the T value is four times less than for the elastic dp scattering. The estimated energy losses for recoil protons from the quasielastic scattering are shown in Fig. 7 (line). One can see that, in the vicinity of $|t| = 0.2$ (GeV/c) 2 , the “thick” counter alone is not helpful in separating elastic dp from quasielastic pp scatterings.

D. Time drift of offsets in setup

The time drift of all offsets was studied with the greatest possible accuracy. The TOF system and ΔE - E counters proved to be stable. The offsets of wire and straw chambers showed significant time drift. Under these circumstances, the whole data set was divided into 13 time slices, and the offsets were found independently for each of these time slices.

E. Selection of elastic events

The main criteria used to select the elastic events were as follows:

- (i) $|m - m_d| < 5\sigma_m$ for the reconstructed mass of incident particles, where $\sigma_m = 0.038$ GeV/c 2 .
- (ii) The interaction point has to be in hydrogen: $|z_{\text{int}} - z_{\text{wall}}| > 3\sigma_w$, $|x_{\text{int}} - x_{\text{wall}}| > 3\sigma_w$, $\sigma_w = 2.4$ mm.
- (iii) $|(a_s - a'_s)| < 3\sigma_a$, $\sigma_a = 15$ mrad.
- (iv) The energy-losses cut was used in the form

$$\left(\frac{\ln(s_1/s'_1)}{\sigma_{s1}}\right)^2 + \left(\frac{\ln(s_2/s'_2)}{\sigma_{s2}}\right)^2 \leq (2.5)^2,$$

where s_i and s'_i are the measured and expected signals, respectively, from the thin and the thick counter pairs measuring the recoil particle energy losses, and σ_{s_i} is

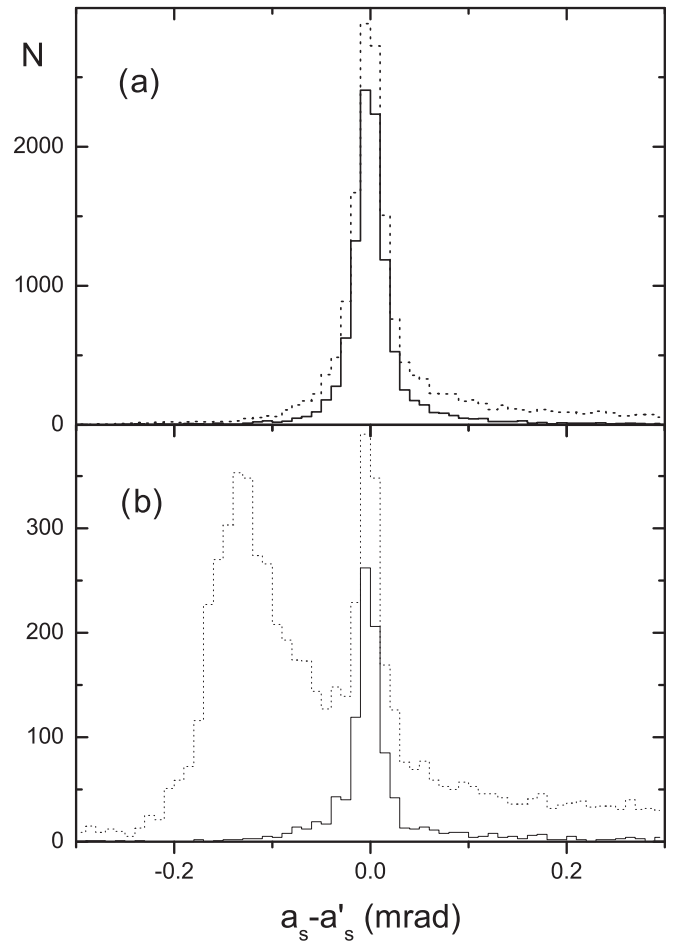


FIG. 8. Elastic peak at $0.08 < |t| < 0.16$ (a) and $0.2 < |t| < 0.3$ (GeV/c) 2 (b) without cuts (dashed histogram) and with ΔE - E cuts (solid histogram).

the halfwidth of the $\ln(s_i)$ distribution for elastic events.

This condition leads to loss of about 5% of good events.

- (v) $0.06 < -t < 0.36$ (GeV/c) 2 .
- (vi) $|\varphi|$ is within the interval 45° to 135° relative to the XZ plane, which corresponds to $\cos 2\varphi \leq 0$.

The selection of elastic events is shown in Fig. 8. After application of the criteria listed above, the background under the elastic peak in each t bin was evaluated. As seen in Fig. 9, where the $(a_s - a'_s)$ distributions for different signs of the beam tensor polarization ρ_{20} are shown for the calibration data, the background level depends on the beam polarization. Therefore, for the background estimation an unpolarized deuteron beam was used. The background was t dependent, changing from 0% to 7.5% with maximum in the vicinity of $-t = 0.2$ (GeV/c) 2 .

The reconstructed differential yields for calibration measurements at 3.39 and 3.77 (GeV/c) 2 are shown in Fig. 10. They are compared with measurements at 3.0 GeV/c from Ref. [17]. Our data were normalized to the fit curve, describing the data from Ref. [17]. One can see that the shape of the differential cross section does not depend upon the deuteron momentum in the region of $p_d \sim 3$ to 3.77 GeV/c.

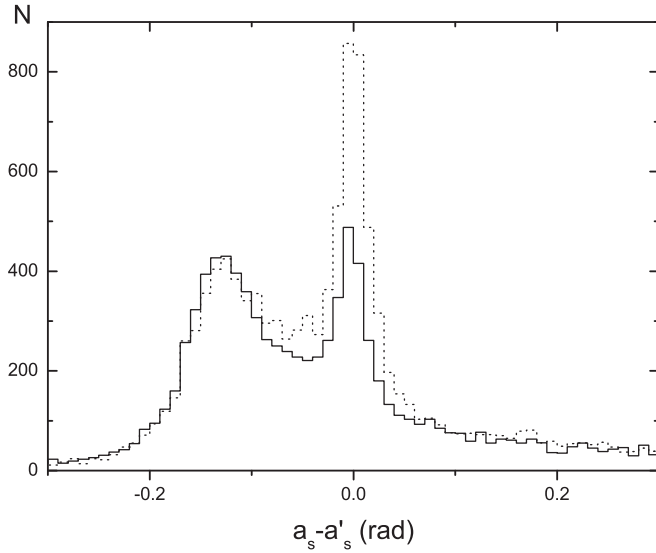


FIG. 9. Elastic peak with background at $0.2 < |t| < 0.3$ (GeV/c)² for $\rho_{20} > 0$ (solid histogram) and for $\rho_{20} < 0$ (dotted histogram) as a function of $a_s - a'_s$ [see Eq. (2)].

The first two points at the lowest $|t|$ are significantly below the curve because of the shrinkage of the effective φ acceptance: recoil particles with small energy and azimuthal angles far from 90° cannot reach the ΔE - E detectors due to the energy losses in the liquid hydrogen, target walls, and straw tubes. Nevertheless, this range of t was used for the determination of the deuteron tensor polarization because, in the ratios of yields (see Secs. IV and V), the acceptance factors cancel.

IV. CALIBRATION MEASUREMENTS

The general form of the cross section for the scattering of polarized deuterons, when the quantization axis is vertical and

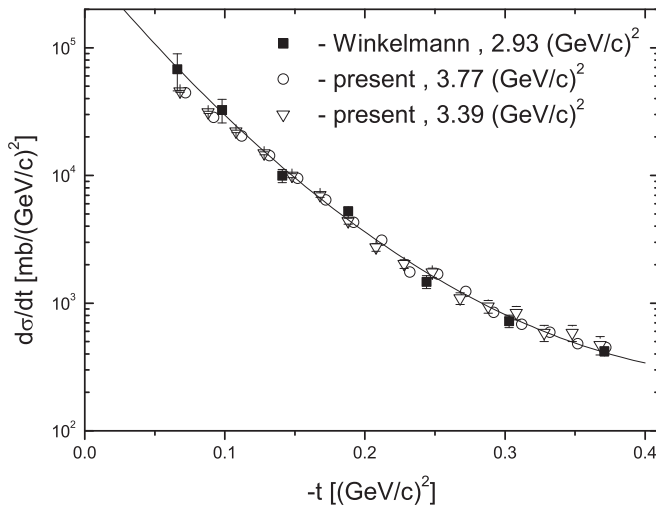


FIG. 10. Differential cross sections for elastic dp scattering. The present data are normalized to fit the curve describing the data from Ref. [17].

in the absence of vector polarization, is as follows [14]:

$$\sigma^\pm = \sigma^0 \left(1 \mp \frac{1}{2} T_{20}(t) |\rho_{20}| \mp \sqrt{\frac{3}{2}} T_{22}(t) \cos 2\varphi |\rho_{20}| \right). \quad (5)$$

It can be transformed to the asymmetry

$$R(t, \varphi) = \frac{\sigma^+ - \sigma^-}{\sigma^+ + \sigma^-} = -\frac{1}{2} T_{20}(t) |\rho_{20}| - \sqrt{\frac{3}{2}} T_{22}(t) \cos 2\varphi |\rho_{20}|. \quad (6)$$

The experimental event distributions in the $(t, \cos 2\varphi)$ plot were analyzed with bin sizes $\Delta t = 0.02$ (GeV/c)² and $\Delta \cos 2\varphi = 0.1$.

The statistics within the available φ interval was not enough to determine independently both T_{20} and T_{22} . To evaluate these values, the following method was used, which was motivated by the independence of the differential cross-section shape with respect to the beam momentum in the interval 3 to 3.77 GeV/c. First, a parametrization of the data [10] at 2.93 GeV/c by a fifth-degree polynomials was used for $T_{20}(t)$ and $T_{22}(t)$. Next, the data of the calibrating measurements were fit with the form

$$\sum_{i,j} \frac{1}{\delta_{ij}^2} [R_{i,j}^{\text{expt}} - R(t_i, \cos 2\varphi_j)]^2 = \min, \quad (7)$$

using a parametrized form of the analyzing powers T_{20} and T_{22} from [10]. Here, δ_{ij} are the experimental uncertainties.

The experimental values R^{expt} in Eq. (7) were taken in the form

$$R^{\text{expt}} = \frac{a_{\text{as}}(\sigma^5 + \sigma^6) - (\sigma^7 + \sigma^8)}{a_{\text{as}}(\sigma^5 + \sigma^6) + (\sigma^7 + \sigma^8)}, \quad (8)$$

where σ^m are yields, obtained for Hyperion mode m ($m = 5$ to 8) and normalized by scintillator monitors ($FH \wedge S_1 \wedge S_2$). As is obvious from Table I, this asymmetry can depend only on the tensor polarization of the beam.

The parameter a_{as} was introduced to evaluate the instrumental asymmetry in these measurements. The source of this asymmetry is the different setup dead time for different tensor polarization modes (the monitor was not gated by the setup dead time). This parameter helps satisfy the conditions $R(t, \varphi) \rightarrow 0$ at $t \rightarrow 0$. The quantities $|\rho_{20}|$ (Eq. (6)) and a_{as} were free parameters in the fit following Eq. (7).

The fit resulted in values of $|\rho_{20}| = 0.535 \pm 0.027$ and 0.525 ± 0.035 at 3.77 and 3.39 GeV/c, respectively, with $a_{\text{as}} = 0.976 \pm 0.009$ and 0.981 ± 0.009 , respectively.¹

The $|\rho_{20}|$ values obtained agree well (within the error bars) with the results of beam polarization measurements: $|\rho_{20}| = P_{zz}/\sqrt{2} = 0.58 \pm 0.02$ and 0.56 ± 0.03 . Such agreement justifies the assumption that the analyzing powers do not change significantly in the range 2.93–3.77 GeV/c. That allowed us to use the parametrization of the data from Ref. [10] up to 3.77 GeV/c.

¹The values of a_{as} agree well with expectations, based on the asymmetry of the dA total cross section, arising when the deuteron beam is aligned.

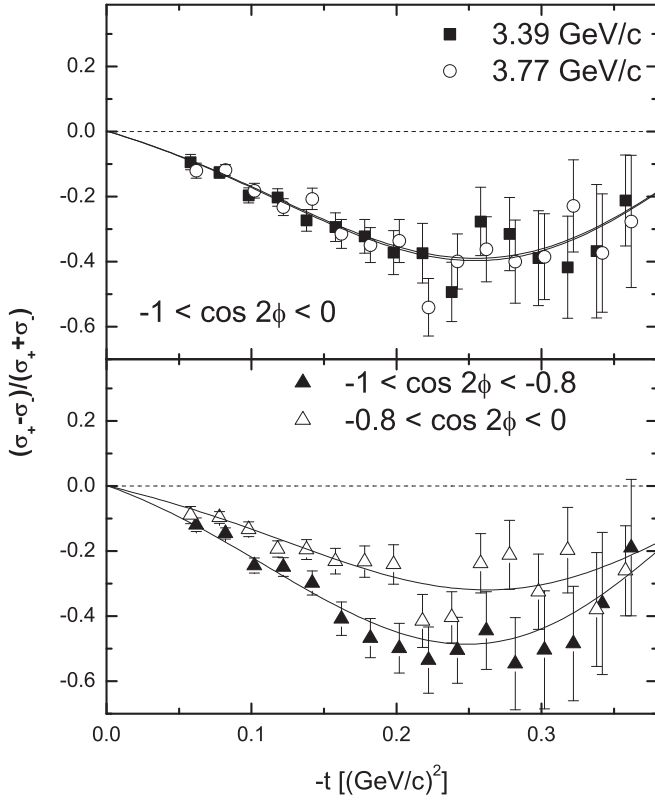


FIG. 11. (a) Asymmetry for the calibrating measurements with the polarized deuteron beam at two momenta. (b) Asymmetry for the joined data in different ranges of φ .

The t dependence of the asymmetry is shown in Fig. 11. It is to be compared with the curves which represent the data of Ref. [10]. In Fig. 11 data at the two momenta used in this experiment have been binned in $-1 < \cos 2\varphi < 0$ intervals. The curve was calculated by substituting the mean value of the $\cos 2\varphi = -0.626$ for this range into Eq. (6).

In Fig. 11(b) the data averaged over these two momenta are grouped within $-1 < \cos 2\varphi < -0.8$ and $-0.8 < \cos 2\varphi < 0$. The mean values for $\cos 2\varphi$ are of -0.93 and -0.58 , respectively.

V. MEASUREMENT OF DEUTERON TENSOR POLARIZATION

The general form of the cross section for the scattering of polarized deuterons, when the quantization axis is longitudinal and in the absence of a vector polarization, can be written as [14]

$$\sigma(t) = \sigma^0(t)[1 + \rho_{20}T_{20}(t)], \quad (9)$$

where the term corresponding to azimuthal asymmetry is absent.

The unpolarized cross section σ^0 was obtained by combining all polarization modes in the form

$$\sigma^0 = \frac{a_{\text{as}}(\sigma^5 + \sigma^6) + \sigma^7 + \sigma^8}{4}, \quad (10)$$

where a_{as} is the coefficient obtained from the fit according to Eqs. (7) and (8). The analyzing power $T_{20}(t)$ [10] was

used in parametrized form as described in the previous section.

The search for the deuteron tensor polarization ρ_{20} was done in two steps. First, the t -dependent cross section σ^0 for unpolarized deuteron scattering was approximated by an exponential form $\exp(P(t))$, where $P(t)$ was taken as a polynomial of power 6, and the coefficients were obtained by minimization of the following functional:

$$\sum_n \frac{1}{\delta_n^2} [\ln(\sigma_n^0) - P(t_n)]^2 = \min.$$

Second, the data on yields of the deuteron scattering at the analyzing target were fit using the approximations found for $\sigma^0(t)$ and $T_{20}(t)$ in Eq. (9):

$$\sum_n \frac{1}{\delta_n^2} \left[\frac{a\sigma_n - e^{P(t_n)}}{e^{P(t_n)}} - \rho_{20}T_{20}(t_n) \right]^2 = \min. \quad (11)$$

The factor a ensures fulfillment of the condition $\rho_{20}T_{20}(t) \rightarrow 0$ at $t \rightarrow 0$ because corrections of monitor numbers for dead time and calculation of the efficiency at the different time intervals are not precise enough for the accuracy required for the yield normalization. This parameter has the same meaning as a_{as} in Eq. (10).

The mean value of χ^2/NDF using Eq. (11) was 0.8. The normalization factors a differ from 1 by a few percent.

The results for $\rho_{20}T_{20}$ are presented in Fig. 12. The experimental points are asymmetries $[a\sigma_i - \exp(P(t_i))]/\exp(P(t_i))$ (with the values of a found as explained above), and the curves are $\rho_{20}T_{20}(t)$ with the values of ρ_{20} obtained.

VI. RESULTS

To transform the measured deuteron momenta to the internal momentum of the deuteron in ${}^3\text{He}$, we assume that the internal momentum is the so-called light front variable k , defined in [18]. When the transverse deuteron momentum is negligibly small in comparison with the total deuteron momentum, k is related to the fragment momentum q in the fragmented nucleus rest frame as follows [18]:

$$k = \left(\alpha - \frac{1}{2} \right) M_{sf} - \frac{m_s^2 - m_f^2}{2M_{sf}}, \quad (12)$$

where

$$\alpha = \frac{\sqrt{m_s^2 + q^2} + q}{M},$$

$$M_{sf}^2 = \frac{m_s^2(1 - \alpha) + m_f^2\alpha}{\alpha(1 - \alpha)},$$

where m_s is the mass of the spectator, m_f is the mass of its partner (in the general case of a bound or unbound subsystem), and M is the mass of the projectile. In our case the partner (a proton) has fixed mass and calculation of the k value is straightforward.

The data obtained in this experiment are compared with a theoretical prediction based on the PWIA [7]. The parametrization used for the S and D waves [19] of the projection of the ${}^3\text{He}$ wave function onto the $(d + p)$ vertex was obtained by

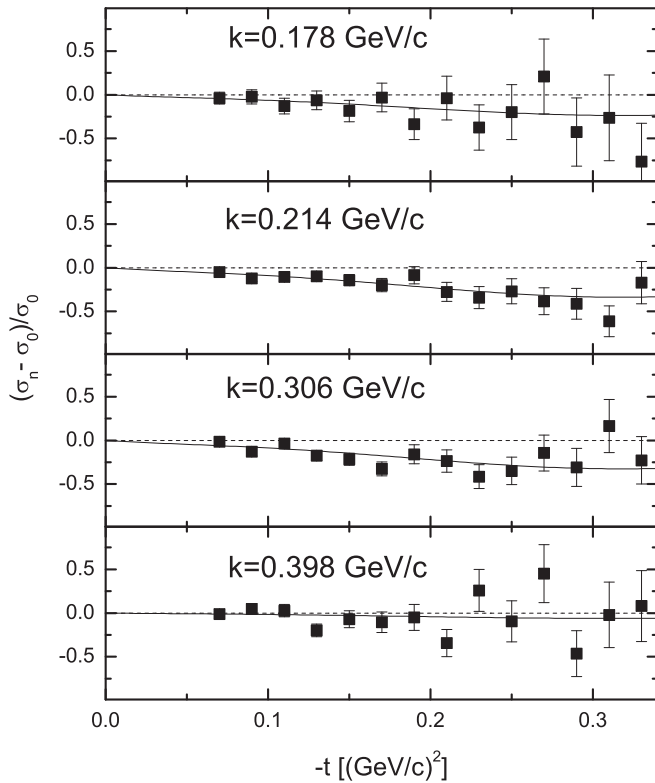


FIG. 12. Asymmetry for different internal momenta of deuteron in ${}^3\text{He}$ [see Eq. (11)].

interpolation from the table of Ref. [20]. With the definition used for the S and D waves from Ref. [19], the expression for the deuteron tensor polarization has the form²

$$\rho_{20}(k) = -\frac{2\psi_S(k)\psi_D(k) + \frac{1}{\sqrt{2}}\psi_D^2(k)}{\psi_S^2(k) + \psi_D^2(k)}. \quad (13)$$

The experimental values of $\rho_{20}(k)$ are given in Table II and shown in Fig. 13(a) (solid squares) together with the PWIA curve [7]. One can see that the data agree well with this prediction for $k < 0.2$ GeV/c. A similar situation occurs with T_{20} in the ${}^1\text{H}(\vec{d}, p)X$ reaction (open circles), where deviation from PWIA starts also from $k = 0.2$ GeV/c. The comparison with T_{20} in backward dp elastic scattering [21,22] (solid and open triangles) is given in order to discuss an eventual zero crossing of the investigated polarization observable. The present data hardly confirm the zero crossing. The experience gained from backward dp elastic scattering indicates that the extrapolation of the data from the experimental points at $k < 0.6$ GeV/c showed a trend which could justify an extrapolation to zero and to positive values, while the following experiments at $k > 0.6$ GeV/c did not confirm this trend.

The deviation of the present experimental data at $k > 0.2$ GeV/c, when compared with the prediction based on

²Due to small angular acceptance of SPES-4, we have $-t \leq 0.02$ (GeV/c)² for quasielastic dp scattering, which is shown in Fig. 1(b). In this region both T_{20} and T_{22} are negligible, so the deuteron alignment stays unchanged.

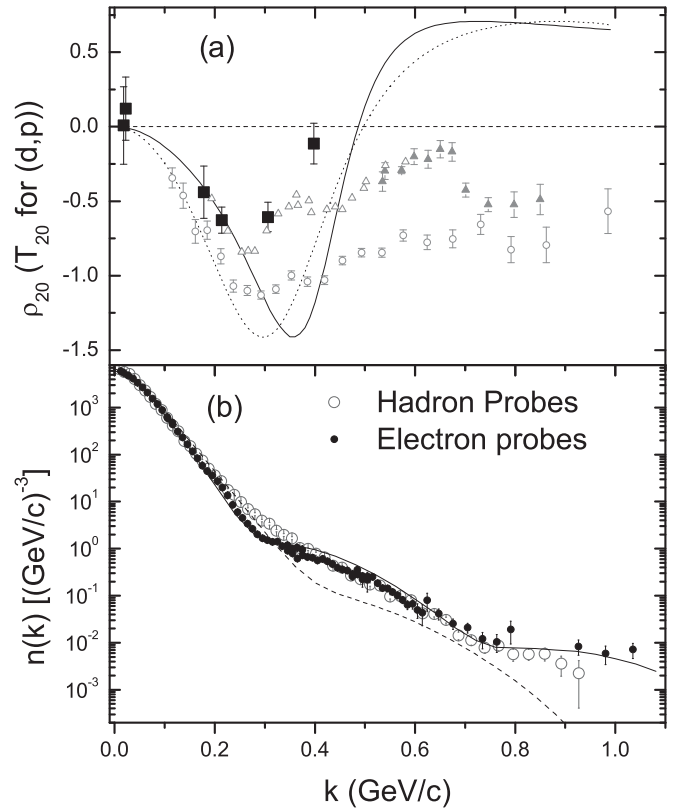


FIG. 13. (Color online) (a) Deuteron tensor polarization versus its internal momentum in ${}^3\text{He}$ (solid squares). The solid line is a prediction from Ref. [7]. Open gray circles are T_{20} data in the ${}^1\text{H}(\vec{d}, p)X$ reaction from Ref. [5] and dashed line is a PWIA calculation for this reaction. Open and solid gray triangles are T_{20} data for ${}^1\text{H}(\vec{d}, p)d$ reaction from Refs. [21] and [22], respectively. (b) Momentum distribution of deuterons in ${}^3\text{He}$ obtained from Ref. [3] (open red circles) and Ref. [23] (solid black circles). The curves are taken from Ref. [24]; here the dashed line is from a PWIA calculation and the solid line is from a PWIA + FSI calculation.

Eq. (13), is similar to the discrepancy observed with the deuteron momentum distributions in ${}^3\text{He}$, obtained with various probes and shown in Fig. 13(b); the data obtained with the hadron probe [3] are shown together with recent data from a Jefferson Laboratory Hall A experiment [23]. In the kinematics used in [23], the missing momentum $p_m \simeq k$ is actually the transverse momentum of the deuteron in ${}^3\text{He}$. The data [23] as well as the calculation from Ref. [24] were scaled by a common factor to compare their k dependence with the data obtained from [3]. It is seen that both data sets agree well except in a small region in the vicinity of $k = 0.3$ GeV/c. The data obtained with the electron probe are well described by the PWIA including a correction for final state interaction (FSI) with the AV18 potential [25]. The predominance of the PWIA at $k < 0.2$ GeV/c is manifest, and the ${}^3\text{He}$ data presented here confirm this predominance. Our point at the highest value of k might require the inclusion of FSI contributions with the same model of the ${}^3\text{He}$ nucleus wave function. But the data point at $k = 0.305$ GeV/c is the most difficult to explain; it is situated in the region of maximum

discrepancy between electron and hadron probe cross section data. There may be other reasons for the disagreement from PWIA expectations, based on the existing models of the ^3He nucleus wave function, similar to effects found in the deuteron case [4,6]. In that case none of the existing theoretical models can provide a good self-consistent description of the cross sections and spin-dependent observables simultaneously at the present time. It is likely that some additional mechanisms, like the one considered in Ref. [8], with rescattering of an intermediate pion, may be required to describe both the momentum distribution [3] and ρ_{20} data in the vicinity of $k = 0.3 \text{ GeV}/c$.

VII. CONCLUSIONS

The deuteron tensor polarization in the $^1\text{H}(^3\text{He}, \vec{d})X$ reaction has been measured in the internal momentum range 0 to 0.4 GeV/c . Up to $k < 0.2 \text{ GeV}/c$ the data agree well with the PWIA approach. At higher values of k one might expect a good description within the framework of the PWIA + FSI model, possibly including some additional mechanism, although none is available presently. These data show that polarization observables add unique experimental information and should stimulate theoretical efforts for a better understanding of the light nuclei structure.

ACKNOWLEDGMENTS

The idea of this experiment was elaborated with the help of M. P. Rekaló, who developed the theoretical background, and who passed away in 2004.

The authors are indebted to M. Garçon for a number of suggestions for improving the experiment.

The authors are grateful to the staff of the SATURNE-II accelerator, Saclay, for the production of excellent beams of ^3He and tensor polarized deuterons. The contribution of L. S. Azhgirey and D. A. Kirillov to the analysis phase of this experiment is gratefully acknowledged. We appreciate the contribution of L. Pentchev, Yu. A. Plis, and R. Abegg to the proposal of this experiment. We are grateful to L. P. Kaptari and Yu. N. Uzikov for fruitful discussions of the results presented here.

The work was supported in part by the US National Science Foundation (PHY91-11942) and the US Dept. of Energy (DE-FG05-90ER40525).

APPENDIX: MEASUREMENT OF RECOIL PROTON ANGLE PROJECTION

In order to achieve a reliable separation of elastic dp events in the analyzing target from the background, a very good resolution on the recoil angle projection is necessary. To reach this goal a specific reconstruction algorithm has been developed.

Parameters of the recoil tracks, $z = a_s y + b_y$, in the 4 (3 + 1) straw planes were searched in form

$$\sum_{i=1}^4 \left(\frac{|a_s y_i + b_y - z_{ji}|}{1 + a_s^2} - r_{ji} \right)^2 = \min. \quad (\text{A1})$$

Here z_{ji} is the z coordinate of the j th tube central wire of the i th plane. It was used in the form

$$\begin{aligned} z_{ji} &= (j - 1)D \quad (i > 1), \\ z_{j1} &= (j - 1)D + c_t x \quad (i = 1), \end{aligned} \quad (\text{A2})$$

where D is the tube diameter. The coefficient c_t takes into account the xz inclination between the first and (2–4) planes, because they were mounted independently. The value of x in Eq. (A2) was not known *a priori* so, in the first step, it was assumed that $x = 0$; then the interaction point was reconstructed using Eqs. (1)–(3) and the next step was performed with the x value found in the previous set.

The distance between the track and the cylindrical drift tube central wire was calculated from

$$r_{ji} = c_{ji} + c_t t_d + c_q t_d^2, \quad (\text{A3})$$

where t_d is a drift time in TDC units. The c_{ji} parameters were used taking into account their time drift (see Sec. III D).

The angles of relative rotation of straws with respect to the wire chamber system were found by fitting the elastic peak. The zy rotation moves it to the correct position (0), and the zx rotation makes it a little bit narrower.

All these rotations are within 3 mrad with an accuracy of about 1 mrad.

The track reconstruction and global search of parameters was carried out with the help of the modified FUMILI package [26]. The method of parameter search was based on a comparison of the distance between the track and the drift tube central wire for each tube in the i th plane with the predicted value obtained by the track reconstruction excluding this plane. This bootstrap process converges after three to four steps.

-
- [1] P. Kitching, G. A. Moss, W. C. Olsen, W. J. Roberts, J. C. Alder, W. Dollhopf, W. J. Kossler, C. F. Perdrisat, D. R. Lehman, and J. R. Priest, *Phys. Rev. C* **6**, 769 (1972).
 [2] M. B. Epstein *et al.*, *Phys. Rev. C* **32**, 967 (1985).
 [3] V. G. Ableev, D. V. Anchishkin, Kh. Dimitrov, S. A. Zaporozhets, A. P. Kobushkin, L. V. Malinina, A. A. Nomofilov, N. M. Piskunov, I. M. Sitnik, and E. A. Strokovsky, *JETP Lett.* **45**, 596 (1987).
 [4] V. G. Ableev *et al.*, *Nucl. Phys. A* **393**, 491 (1983); **411**, 541 (1983); V. Punjabi *et al.*, *Phys. Rev. C* **39**, 608 (1989); V. G.

- Ableev *et al.*, *JINR Rapid Comm.* **1[52]–92**, 10 (1992); T. Aono *et al.*, *Phys. Rev. Lett.* **74**, 4997 (1995).
 [5] L. S. Azhgirey *et al.*, *Phys. Lett. B* **387**, 37 (1996).
 [6] B. Kuhn, V. P. Ladygin, P. K. Manyakov, N. M. Piskunov, I. M. Sitnik, E. A. Strokovsky, L. Penchev, and A. P. Kobushkin, *Phys. Lett. B* **334**, 298 (1994).
 [7] I. M. Sitnik, V. P. Ladygin, L. Penchev, N. M. Piskunov, E. A. Strokovsky, Yu. A. Plis, M. P. Rekaló, C. F. Perdrisat, V. Punjabi, and R. Abegg, *JINR preprint E1-94-186* (1994).
 [8] Y. Shimizu *et al.*, *Phys. Rev. C* **76**, 044003 (2007).

- [9] E. Tomasi-Gustafsson, I. M. Sitnik, C. F. Perdrisat, and M. P. Rekalo, *Nucl. Instrum. Methods Phys. Res., Sect. A* **402**, 361 (1998); E. Tomasi-Gustafsson *et al.*, *ibid.* **420**, 90 (1999).
- [10] V. Ghazikhanian *et al.*, *Phys. Rev. C* **43**, 1532 (1991).
- [11] E. Grorud, J. L. Laclare, A. Ropert, A. Tkatchenko, J. Banaigs, and M. Boivin, *Nucl. Instrum. Methods* **188**, 549 (1981).
- [12] L. B. Golovanov, Yu. Borzunov, N. M. Piskunov, A. P. Tsvinev, J. Ball, J. L. Sans, and E. Tomasi-Gustafsson, *Nucl. Instrum. Methods Phys. Res., Sect. A* **430**, 1 (1999).
- [13] P.-A. Chamouard *et al.*, *J. Phys.* **51**, C6-569 (1990); J.-L. Lemaire, *International Workshop on Polarized Sources and Polarized Gas Jets—1990, Tsukuba, Japan*, Proc. KEK, Report 90-15, edited by Y. Mori, p. 116.
- [14] J. Arvieux, S. D. Baker, A. Boudard, J. Cameron, T. Hasegawa, D. Hutcheon, C. Kerboul, G. Gaillard, and Van Sen Nguyen, *Nucl. Instrum. Methods Phys. Res., Sect. A* **273**, 48 (1988).
- [15] B. Bonin *et al.*, *Nucl. Instrum. Methods Phys. Res., Sect. A* **288**, 379 (1990).
- [16] L. V. Malinina and E. A. Stokovsky, *Part. Nucl. Lett.* **100**, 86 (2000); L. V. Malinina *et al.*, *Phys. Rev. C* **64**, 064001 (2001).
- [17] E. Winkelmann, P. R. Bevington, M. W. McNaughton, H. B. Willard, F. H. Cverna, E. P. Chamberlin, and N. S. P. King, *Phys. Rev. C* **21**, 2535 (1980).
- [18] P. A. M. Dirac, *Rev. Mod. Phys.* **21**, 392 (1949); B. L. G. Bakker, L. A. Kondratyuk, and M. V. Terent'ev, *Nucl. Phys. B* **158**, 497 (1979); H. Leutwyler and J. Stern, *Ann. Phys. (NY)* **112**, 94 (1978); A. P. Kobushkin and V. P. Shelest, *EChAYa* **14**, 1146 (1983); V. A. Karmanov, *ibid.* **19**, 525 (1988).
- [19] J-F. Germond and C. Wilkin, *J. Phys. G* **14**, 181 (1988).
- [20] R. Schiavilla, V. R. Pandharipande, and R. B. Wiringa, *Nucl. Phys. A* **449**, 219 (1986).
- [21] V. Punjabi *et al.*, *Phys. Lett. B* **350**, 178 (1995).
- [22] L. S. Azhgirey *et al.*, *Phys. Lett. B* **391**, 22 (1997).
- [23] M. M. Rvachev *et al.*, *Phys. Rev. Lett.* **94**, 192302 (2005).
- [24] C. Ciofidegli Atti and L. P. Kaptari, *Phys. Rev. Lett.* **100**, 122301 (2008).
- [25] R. B. Wiringa, V. G. J. Stoks, and R. Schiavilla, *Phys. Rev. C* **51**, 38 (1995).
- [26] I. M. Sitnik, JINR preprints E11-2008-43, E11-2010-101.